



1 **I** **ferences of the inverted terrestrial ecosystem carbon flux between using GO-**
2 **SAT and OCO-2 XCO₂ retrievals**

3 Hengmao Wang¹, Fei Jiang^{1,2*}, Jun Wang¹, Weimin Ju¹, Jing M. Chen^{1,3}

4 *1 Jiangsu Provincial Key Laboratory of Geographic Information Science and Technology, International Institute for*
5 *Earth System Science, Nanjing University, Nanjing, 210023, China*

6 *2 Jiangsu Center for Collaborative Innovation in Geographical Information Resource Development and Application,*
7 *Nanjing, 210023, China*

8 *3, Department of Geography, University of Toronto, Toronto, Ontario M5S3G3, Canada*

9

10 **Abstract**

11 In this study, both the Greenhouse Gases Observing Satellite (GOSAT) and the Orbiting Car-
12 bon Observatory 2 (OCO-2) XCO₂ retrievals are assimilated within the GEOS-Chem 4D-Var assim-
13 ilation framework to constrain the terrestrial ecosystem carbon flux during Jul 1, 2014 to Dec 31,
14 2015. The inverted global and regional carbon fluxes during Jan 1 to Dec 31, 2015 are shown and
15 discussed. Surface CO₂ mixing ratios from 47 surface flask sites and XCO₂ measurements from 13
16 TCCON sites are used to evaluate the simulated concentrations with the posteriori carbon fluxes. The
17 results show that globally, the terrestrial ecosystem carbon sink (excluding biomass burning emis-
18 sions) estimated from GOSAT data is stronger than that inferred from OCO-2 data, and the annual
19 atmospheric CO₂ growth rate estimated from GOSAT data is more consistent with the estimate of
20 GCP 2017. Regionally, in most regions, the land sinks inferred from GOSAT data are also stronger
21 than those from OCO-2 data. Compared with the prior fluxes, the carbon fluxes in northern temperate
22 regions change most, followed by tropical and southern temperate regions, and the smallest changes
23 occur in boreal regions. Basically, in temperate regions, the inferred land sinks are significantly in-
24 creased, while those in tropical regions are decreased. The different changes in different regions are
25 mainly related to the spatial coverage and the amount of XCO₂ data in these regions. Compared with
26 CT2016, the inferred carbon sinks are comparable in most temperate regions, but much weaker in

* Corresponding author: Tel.: +86-25-83597077; Fax: +86-25-83592288; E-mail address: jiangf@nju.edu.cn



27 boreal and tropical regions. Evaluations using flask and TCCON observations suggest that GOSAT
28 and OCO-2 data, can effectively improve the carbon flux estimates in the northern hemisphere, while
29 in the southern hemisphere the optimized carbon sinks may be overestimated, especially for GOSAT
30 data.

31 **Keywords:** Terrestrial ecosystem carbon flux, inversion, GOSAT, OCO-2, GEOS-Chem

32

33 1. Introduction

34 Atmospheric inverse modeling is an effective method for quantifying surface carbon fluxes at
35 global and regional scales using the gradient of CO₂ measurements. Inversion studies based on in-
36 situ CO₂ observations agree well on global carbon budget estimates but differ greatly on regional
37 carbon flux estimates and the partitioning of land and ocean fluxes as well, mainly due to the sparse-
38 ness of observations in tropics, southern hemisphere oceans and the majority of continental interiors
39 such as those in South America, Africa, and Boreal Asia (Peylin et al., 2013). Satellite observations
40 offer an attractive means to constrain atmospheric inversions with their extensive spatial coverage
41 over remote regions. Studies have shown that satellite observations, though with lower precision than
42 in-situ measurements, can improve the carbon flux estimates (Rayner and O'Brien, 2001; Pak and
43 Prather, 2001; Houweling et al., 2004; Baker et al., 2006; Chevallier, 2007; Miller et al., 2007; Kady-
44 grov et al., 2009; Hungershofer et al., 2010).

45 Satellite sensors designed specifically to measure atmospheric CO₂ concentrations, have been
46 in operation in recent years. The Greenhouse Gases Observing Satellite (GOSAT) (Kuze et al.,
47 2009), being the first satellite mission dedicated to observing CO₂ from space, was launched in
48 2009. The National Aeronautics and Space Administration (NASA) launched the Orbiting Carbon
49 Observatory 2 (OCO-2) satellite in 2014 (Crisp et al., 2017; Eldering et al., 2017). China's first CO₂
50 monitoring satellite (TanSat) was launched in 2016 (Wang et al., 2017; Yang et al., 2017). These sat-
51 ellites measure near-infrared sunlight reflected from the surface in CO₂ spectral bands and the O₂



52 A-band to retrieve column-averaged dry-air mole fractions of CO₂ (XCO₂), aiming to improving the
53 estimation of spatial and temporal distributions of carbon sinks and sources. A number of inversions
54 have utilized GOSAT XCO₂ retrievals to infer surface carbon fluxes (Takagi et al., 2011; Basu et
55 al., 2013; Maksyutov et al., 2013; Saeki et al., 2013; Chevallier et al., 2014; Deng et al., 2014;
56 Houweling et al., 2015; Deng et al., 2016). Although large uncertainty reductions were achieved
57 for regions which are under-sampled by in-situ observations, these studies didn't give robust re-
58 gional carbon flux estimates. There are large spreads in regional flux estimates in some regions
59 among these inversions. Furthermore, regional flux distributions inferred from GOSAT XCO₂ data
60 are significantly different from those inferred from in-situ observations. For instance, several stud-
61 ies using GOSAT retrievals reported a larger than expected carbon sink in Europe (Basu et al.,
62 2013; Chevallier et al., 2014; Deng et al., 2014; Houweling et al., 2015). The validity of this large
63 Europe carbon sink derived from GOSAT retrievals is in intense debate and efforts to achieve a
64 consensus estimate of Europe carbon sinks are still ongoing (Reuter et al., 2014; Feng et al., 2016;
65 Reuter et al., 2017).

66 Compared with GOSAT, OCO-2 has a higher sensitivity near the surface, much finer footprints
67 and more extended spatial coverage, and thus has the potential to better constrain the surface carbon
68 flux inversion (Eldering et al., 2017). Studies have used OCO-2 XCO₂ data to estimate carbon flux
69 anomalies during recent El Nino events (Chatterjee et al., 2017; Patra et al., 2017; Heymann et al.,
70 2017; Liu et al., 2017). Nassar et al. (2017) applied OCO-2 XCO₂ data to infer emissions from large
71 power plants. Miller et al. (2018) evaluated the potential of OCO-2 XCO₂ data in constraining re-
72 gional biospheric CO₂ fluxes and found that in the current state of development, OCO-2 observa-
73 tions can only provide a reliable constraint on CO₂ budget at continental and hemispheric scales. At
74 present, it is still not clear whether with the improved monitoring capabilities, current OCO-2 ob-
75 servations have a greater potential than GOSAT observations for estimating CO₂ flux at regional or



76 finer scale. It is therefore important to investigate how current OCO-2 XCO₂ data differ from GO-
77 SAT XCO₂ data in constraining carbon budget.

78 In this study, we evaluate the performance of GOSAT and OCO-2 XCO₂ data in constraining
79 terrestrial ecosystem carbon flux. GOSAT and OCO-2 XCO₂ retrievals produced by the NASA At-
80 mospheric CO₂ Observations from Space (ACOS) team are applied to infer monthly terrestrial eco-
81 system carbon sinks and sources from Oct, 2014 to December, 2015, using a 4D-Var scheme based
82 on the GEOS-Chem Adjoint model. Inversion results are evaluated against surface flask CO₂ obser-
83 vations and TCCON XCO₂ measurements. ~~We analyze the differences of inverted terrestrial ecosys-~~
84 ~~tem carbon flux between using two XCO₂ data.~~ The inverted carbon fluxes are also compared with
85 results from other datasets such as CarbonTracker CT2016 (Peters, et al., 2007) and Global Carbon
86 Project (GCP) 2017 (Le Quéré et al., 2018). This paper is organized as follows. Section 2 briefly
87 introduces GOSAT and OCO-2 XCO₂ retrievals and the inversion methodology and settings. Results
88 and discussions are presented in Section 3, and Conclusions are given in Section 4.

89

90 **2. Data and Method**

91 2.1 GOSAT and OCO-2 XCO₂ retrievals

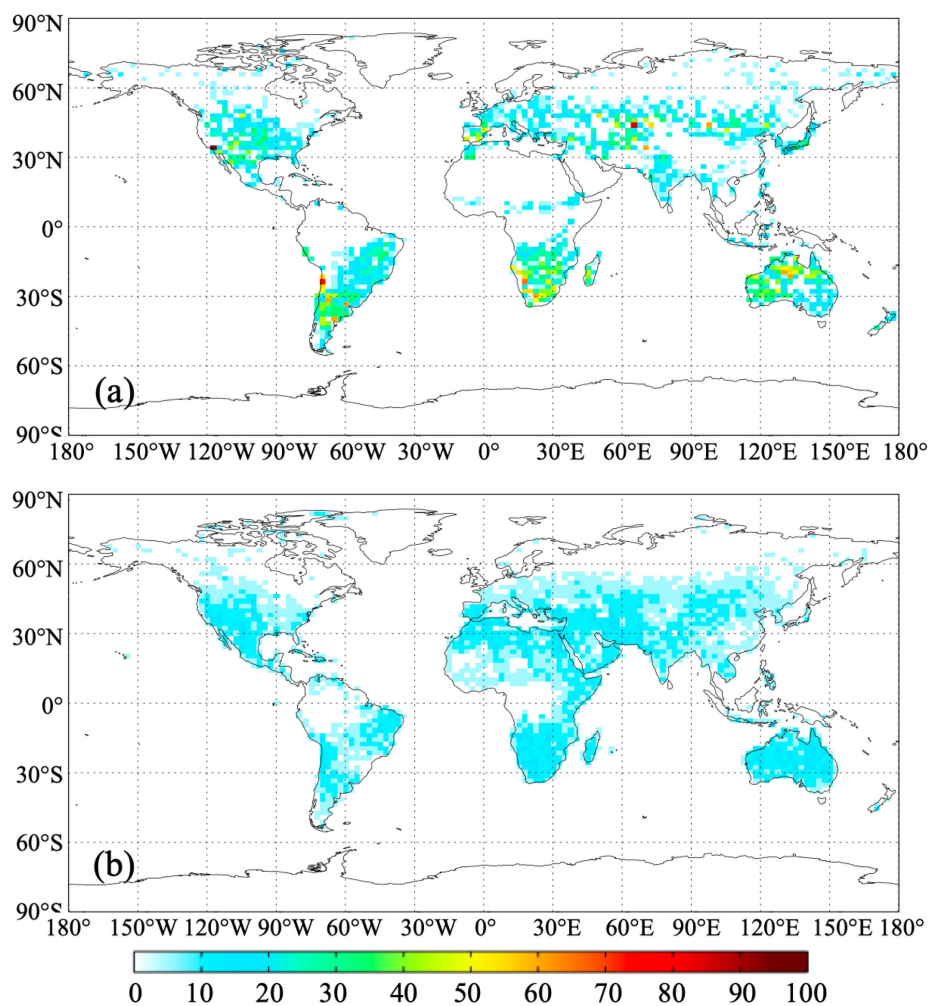
92 Developed jointly by the National Institute for Environmental Studies (NIES), the Japanese
93 Space Agency (JAXA) and the Ministry of the Environment (MOE) of Japan, GOSAT was de-
94 signed to measure total column abundances of CO₂ and CH₄. The satellite flies at a 666 km altitude
95 in a sun-synchronous orbit with 98° inclination that crosses the equator at 12:49 local time. It co-
96 vers the whole globe in three days and has a footprint of 10.5 km² at nadir. OCO-2 is NASA's first
97 mission dedicated to measuring atmospheric CO₂ concentration. It flies at 705 km altitude in a sun-
98 synchronous orbit with an overpass time at approximately 13:30 local time and a repeat cycle of 16
99 days. Its grating spectrometer measures reflected sunlight in three near-infrared regions (0.765, 1.61
100 and 2.06 μm) to retrieve XCO₂. OCO-2 has a footprint of 1.29×2.25 km² at nadir and acquires eight



101 cross-track footprints creating a swath width of 10.3 km.

102 Both GOSAT and OCO-2 XCO₂ products were created using the same retrieval algorithm,
103 which is based on a Bayesian optimal estimation approach (Roggers et. al., 2000; O Dell et. al.,
104 2011). The GOSAT and OCO-2 XCO₂ data used in this study are Version 7.3 Level 2 Lite products
105 at the pixel level. The XCO₂ data from lite products are bias-corrected (Wunch et. al., 2011). Before
106 used in our inversion system, the data are processed in three steps. First, the retrievals for the glint
107 soundings over oceans have relatively larger uncertainty, thus the data over oceans are not used in
108 our inversions (Wunch et. al., 2017). Second, in order to achieve the most extensive spatial cover-
109 age with the assurance of using best quality data available, the XCO₂ data are filtered with two pa-
110 rameters, namely warn_levels and xco2_quality_flag, which are provided along with the XCO₂
111 data. All data with xco2_quality_flag not equaling 0 are removed, the rest are divided into three
112 groups according the value of warn_levels, namely group 1, group 2 and group 3. In group 1, the
113 warn_levels are less than 8, in group 2, the warn_levels are greater than 9 and less than 12, and in
114 group 3, those are greater than 13. Group 1 has the best data quality, followed by group 2, and
115 group 3 is the worst. Third, the pixel data are averaged within the grid cell of 2°×2.5°, which is the
116 resolution of the global atmospheric transport model used in this study. In each grid of 2°×2.5°,
117 only the groups of best data quality are selected and then averaged. The other variables like column
118 averaging kernel, retrieval error and so on which are provided along with the XCO₂ product are also
119 dealt with the same method. Figures 1a and 1b show the coverages and data amount of GOSAT
120 and OCO-2 XCO₂ data during the study period after processing.

121



122

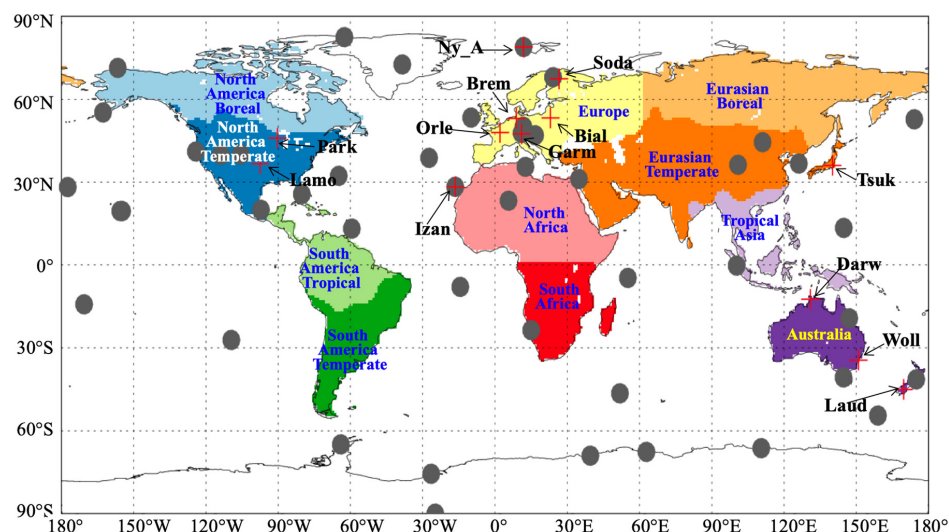
123 **Figure 1.** Data amount of each grid cell (2°x2.5°) of ACOS XCO₂ used in this study (a, GOSAT; b,
124 OCO-2)

125 2.2 Surface flask and TCCON CO₂ measurements

126 We evaluate the inversion results through comparing the modeled CO₂ mixing ratios using the
127 posteriori fluxes with surface flask measurements and Total Carbon Column Observing Network
128 (TCCON) XCO₂ observations. The flask measurements of CO₂ mixing ratios are downloaded from
129 World Data Center for Greenhouse Gases (WDCGG) under the World Meteorological Organization
130 (WMO) Global Atmospheric Watch (GAW) programme (<http://ds.data.jma.go.jp/gmd/wdcgg/>). 47



131 surface sites which have valid observations for at least two months in 2015 are chosen. TCCON is a
132 network of ground-based Fourier Transform Spectrometers that measure direct near-infrared solar
133 absorption spectra. Column-averaged abundances of atmospheric constituents including CO₂, CH₄,
134 N₂O, HF, CO, H₂O, and HDO are retrieved through these spectra. We use XCO₂ retrievals from 13
135 stations from TCCON GGG2014 dataset (Blumenstock et al., 2017; Deutscher et al., 2017; Griffith
136 et al., 2017a, b; Kivi et al., 2017; Morino et al., 2017; Notholt et al., 2017a, b; Sherlock et al., 2017;
137 Sussmann and Rettinger, 2017; Warneke et al., 2017; Wennberg et al., 2017a, b). The locations of
138 47 flask sites and 13 TCCON stations are shown in Figure 2.



139
140 **Figure 2.** Distributions of the 47 surface flask sites (gray solid circle) and 13 TCCON sites (red
141 cross mark), shaded shows the 11 TRANSKOM regions

142 2.3 GEOS-Chem 4DVAR assimilation framework

143 In this work, bias-corrected XCO₂ retrievals are assimilated to estimate monthly terrestrial eco-
144 system carbon fluxes using the GEOS-Chem and its adjoint model in a 4D-Var assimilation frame-
145 work.

146 2.3.1 GEOS-Chem model

147 GEOS-Chem model (<http://geos-chem.org>) is a global three-dimensional chemistry transport



148 model (CTM), which is driven by assimilated meteorological data from the Goddard Earth Observ-
149 ing System (GEOS) of the NASA Global Modeling and Assimilation Office (GMAO) (Rienecker et
150 al., 2008). The original CO₂ simulation in the GEOS-Chem model was developed by Suntharalin-
151 gam *et al.* (2004) and accounts for CO₂ fluxes from fossil fuel combustion and cement production,
152 biomass burning, terrestrial ecosystem exchange, ocean exchange and biofuel burning. Nassar et al.
153 (2010) updated the CO₂ simulation with improved inventories. In addition to the inventories in ear-
154 lier version, the new CO₂ fluxes includes CO₂ emissions from international shipping, aviation (3D)
155 and the chemical production of CO₂ from CO oxidation throughout the troposphere. In most other
156 models, the oxidation of CO was treated as direct surface CO₂ emissions. The details of the CO₂
157 simulation and the CO₂ sinks/sources inventories could be found in Nassar et al. (2010). The ver-
158 sion of GEOS-Chem model used in this study is v8-02-01.

159 2.3.2 GEOS-Chem adjoint model

160 An adjoint model is used to calculate the gradient of a response function of one model scalar
161 (or cost function) with respect to a set of model parameters. The adjoint of the GEOS-Chem model
162 was first developed for inverse modeling of aerosol (or their precursors) and gas emissions (Henze
163 et al., 2007). It has been implemented to constrain sources of species such as CO, CH₄, and O₃ with
164 satellite observations (Kopacz et al., 2009, 2010; Jiang et al., 2011; Wecht et al., 2012; Parrington et
165 al., 2012). Several studies have successfully used this adjoint model to constraint carbon sources
166 and sinks with surface flask measurements of CO₂ mixing ratio and space-based XCO₂ retrievals
167 (Deng et al., 2014; Liu et al., 2014; Deng et al., 2016; Liu et al., 2017).

168 2.3.3 Inversion method

169 In the GEOS-Chem inverse modeling framework, the 4D-Var data assimilation technique is
170 employed for combining observations and simulations to seek a best optimal estimation of the state
171 of a system. This approach seeks the scaling factors of the carbon flux that minimize the cost func-
172 tion, J , given by:



$$173 \quad J(c) = \frac{1}{2} \sum_{i=1}^N (XCO_{2,i}^m - XCO_{2,i}^{obs}) S_{obs,i}^{-1} (XCO_{2,i}^m - XCO_{2,i}^{obs}) + \frac{1}{2} (c - c_a) S_c^{-1} (c - c_a)$$

174 where N is total number of satellite XCO_2 observations; XCO_2^m and XCO_2^{obs} are modeled and ob-
 175 served total column averaged dry air mole fraction of CO_2 respectively; c_a is the priori scaling factor
 176 of the carbon flux, which is typically set as unity; S_{obs} is the model-data mismatch error covariance
 177 matrix; S_c is the scaling factor error covariance matrix. The gradients of the cost function with re-
 178 spect to scaling factors calculated with the adjoint model are supplied to an optimization routine
 179 (the L-BFGS-B optimization routine; Byrd et al., 1995; Zhu et al., 1994), and the minimum of the
 180 cost function is sought iteratively.

181 For the modeled CO_2 column to be comparable with the satellite XCO_2 retrievals, the modeled
 182 CO_2 concentration profile should be first mapped into the satellite retrieval levels and then convo-
 183 luted with retrieval averaging kernels. The modeled XCO_2 is computed by:

$$184 \quad XCO_2^m = XCO_2^a + \sum_j h_j a_j (A(x) - y_{a,j})$$

185 where j denotes retrieval level, x is the modeled CO_2 profile; $A(x)$ is a mapping matrix; XCO_2^a is a
 186 priori XCO_2 , h_j is pressure weighting function, a_j is the satellite column averaging kernel and y_a is
 187 the priori CO_2 profile for retrieval.

188 3. Inversion settings

189 In this study, the GEOS-Chem model was run in a horizontal resolution of $2^\circ \times 2.5^\circ$ for 47 verti-
 190 cal layers. Two experiments, one with GOSAT data and the other with OCO-2 data, were conducted
 191 from Oct 1, 2014 to December 31, 2015. The posteriori dry air mole fraction of CO_2 of Oct 1, 2014
 192 from CT2016 product was taken as the initial concentration. The first three months were taken as
 193 the spin-up period. The priori carbon fluxes used in this study include: fossil fuel and cement manu-
 194 facture CO_2 emissions from the Carbon Dioxide Information Analysis Center (CDIAC) (Andres et



195 al., 2011), biomass burning CO₂ emissions from the Global Fire Emissions Database version 4.1
196 (GFEDv4) (van der Werf et al., 2010; Giglio et al., 2013); terrestrial ecosystem carbon exchanges
197 from the Carnegie-Ames-Stanford Approach (CASA) model GFED4.1 simulation (Potter et al.,
198 1993; van der Werf et al., 2010); CO₂ exchanges over the ocean surface from the posteriori air-sea
199 CO₂ flux from CT2016 (Peters *et al.* 2007, with updates documented at [http://carbon-](http://carbon-tracker.noaa.gov)
200 [tracker.noaa.gov](http://carbon-tracker.noaa.gov)); monthly shipping emissions of CO₂ from the International Comprehensive
201 Ocean–Atmosphere Data Set (ICOADS) (Corbett and Koehler, 2003; Endresen et al., 2004, 2007);
202 3-D aviation CO₂ emissions (Kim et al., 2007; Wilkerson et al., 2010); and 3-D chemical produc-
203 tion of CO₂ from the oxidation of other atmospheric carbon species and its surface corrections (Nas-
204 sar et al., 2010). It is noted that the terrestrial ecosystem CO₂ exchanges, fossil fuel and cement
205 manufacture emissions and biomass burning emissions in our inversions are the same as those in
206 CT2016. Since we exclude XCO₂ retrievals over ocean, in our inversions, the terrestrial ecosystem
207 exchanges might compensate for the under-constrained ocean CO₂ fluxes. To mitigate the impact of
208 the lack of XCO₂ observations over ocean, we directly use the posteriori ocean CO₂ fluxes of
209 CT2016, which were well constrained with surface flask observations at ocean sites. Only terres-
210 trial ecosystem CO₂ exchanges are optimized in our inversions.

211 An efficient computational procedure for constructing non-diagonal priori flux error covariance
212 matrix which accounts for the spatial correlation of errors is implemented (Single et al, 2011). The
213 construction is based on the assumption of exponential decay of error correlations. Other than form-
214 ing covariance matrix explicitly, multiple-dimensional correlations are represented by tensor prod-
215 ucts of one dimensional correlation matrices along longitude and latitudinal directions. For the two
216 inversions, the scale lengths assigned along longitudinal and latitudinal directions are 500 km and
217 400 km for terrestrial ecosystem exchange and 1000 km and 800 km for ocean exchange, respec-
218 tively. No correlations between different types of fluxes are assumed. The temporal correlations are
219 also neglected. Global annual uncertainty of 100% and 40% are assigned for terrestrial ecosystem



220 and ocean CO₂ exchanges, respectively (Deng and Chen, 2011). Accordingly, the ratios of uncer-
221 tainty to the priori land and ocean fluxes in each month at the grid cell level are assigned with 5 and
222 3, respectively.

223 The observation error covariance matrix is constructed using the retrieval error, which is pro-
224 vided along with the XCO₂ data. Observation errors are assumed to be uncorrelated at model grid
225 level. To account for the correlated observation errors, as shown in section 2.1, the pixel level re-
226 trieval errors are filtered and averaged to model at the grid level, and then inflated by a factor of 1.9
227 to ensure the chi-square testing of χ^2 value to be close to 1 (Tarantola, 2004; Chevallier et al.,
228 2007).

229 4. Results and Discussions

230 4.1 Global carbon budget

231 Table 1 presents the optimized global carbon budgets by the two experiments in 2015. For com-
232 parison purposes, the prior fluxes used in this study and the estimates of CT2016 and GCP2017 are
233 also shown in Table 1. The optimized global land sinks based on GOSAT and OCO-2 XCO₂ retriev-
234 als are -3.48 and -2.94 PgC yr⁻¹, respectively, which are larger than the prior value, but lower than
235 the CT2016 estimate based on the flask/in-situ CO₂ concentration observations. The differences of
236 ocean fluxes among a priori and two inversions are small since we don't assimilate XCO₂ data over
237 ocean. GCP gives a comprehensive estimate for the global carbon budget every year. In the GCP
238 2017 estimates, the components of the global carbon budget include fossil fuel and industry, land-
239 use change emissions, atmospheric growth, ocean sink, land sink, and budget imbalance, which are
240 different from those in this study and CT2016 (Table 1). For ease of comparison, the budget imbal-
241 ance, land sink and land-use change emissions are combined as land net flux, and then the biomass
242 burning emissions and the land sink in this study and those from CT2016 are combined to obtain
243 the land net flux. As shown in Table 1, the prior estimate gives the smallest net land flux (-0.5 Pg C
244 yr⁻¹), and the CT2016 estimate is the largest (-1.7 PgC yr⁻¹). The land net flux optimized based on



245 GOSAT and OCO-2 XCO₂ retrievals fall in between (-0.74 and -1.28 PgC yr⁻¹, respectively), and
 246 are much closer to the estimate of GCP 2017 (-1.03 PgC yr⁻¹). A global net flux from GCP is in-
 247 ferred from the global annual atmospheric carbon growth rate, which represents relatively accu-
 248 rately the net carbon flux added into atmosphere. It could be found that the global net flux esti-
 249 mated based on GOSAT data is the closest to the GCP estimate, while the one estimated using
 250 OCO-2 data is higher and the CT2016 estimate is much lower than the GCP result, indicating that
 251 the land and ocean carbon uptakes in CT2016 were overestimated, while those optimized using
 252 OCO-2 data might be underestimated.

253 **Table 1.** Global carbon budgets estimated by the OCO-2 experiment, GOSAT experiment in this
 254 study as well as those from the priori fluxes, CT2016 and GCP2017 (PgC yr⁻¹)

	Priori	OCO-2 ex- periment	GOSAT ex- periment	CT2016	GCP2017
Fossil fuel and industry	9.83	9.83	9.83	9.83	9.83
Biomass burning emissions	2.2	2.2	2.2	2.2	1.52 ^{a)}
Land sink	-2.5	-2.94	-3.48	-3.9	-2.55 ^{b)}
Land net flux	-0.5	-0.74	-1.28	-1.7	-1.03
Ocean sink	-2.41	-2.43	-2.45	-2.41	-2.57
Global net flux	7.12	6.66	6.1	5.72	6.23 ^{c)}

255 ^{a)} land-use change emissions in GCP2017

256 ^{b)} land sink plus budget imbalance

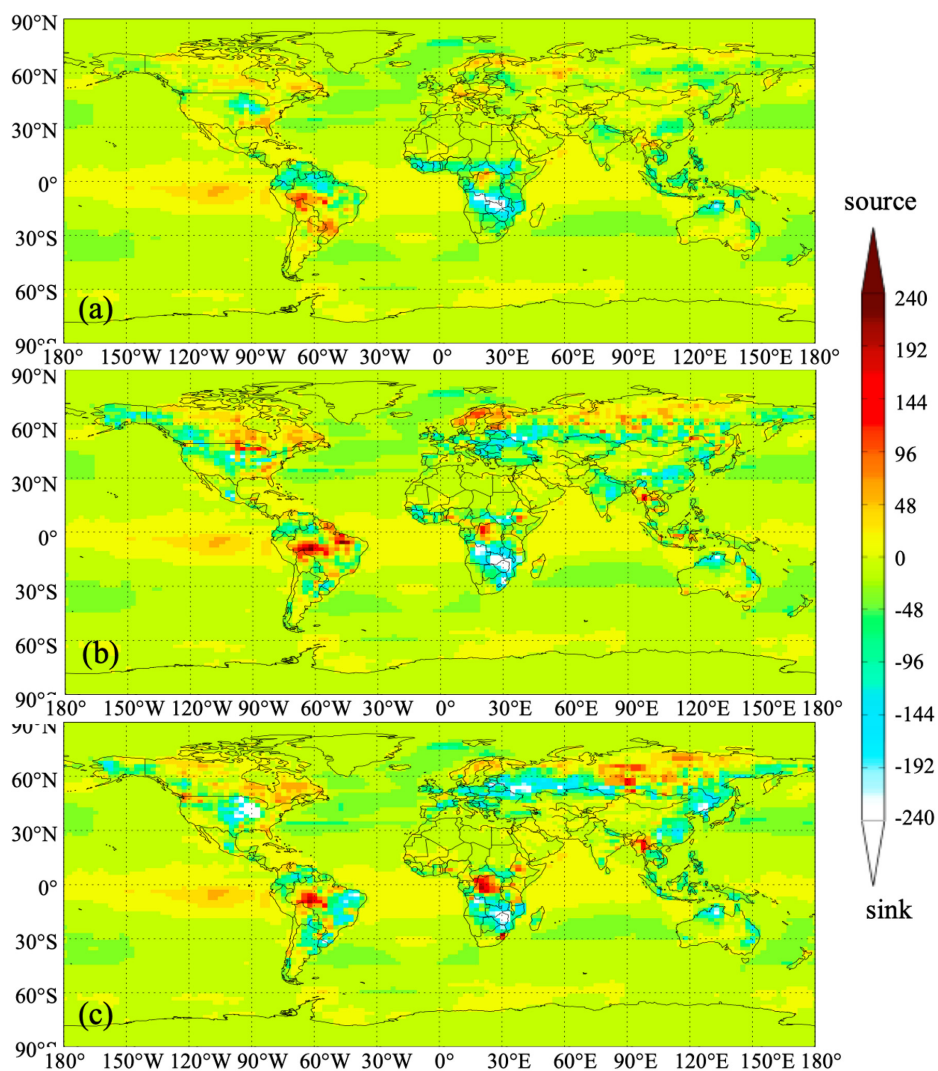
257 ^{c)} atmospheric growth

258 4.2 Regional carbon flux

259 Figure 3 shows the distributions of annual land and ocean carbon fluxes (excluding fossil fuel
 260 and biomass burning carbon emissions, same thereafter) of the prior and the estimates using GOSAT
 261 and OCO-2 data. It could be found that compared with the prior fluxes, the carbon sinks in Central
 262 America, south and northeast China, east and central Europe, south Russia and east Brazil are obvi-
 263 ously increased in GOSAT inversion. Except for east Brazil, the land sinks in those areas in OCO-2
 264 inversion are also increased, but much weaker than those in GOSAT inversion, and in east Brazil, it



265 turns to a significant carbon source. In contrast, in east and central Canada, north Russia, north Eu-
266 rope, west Indo-China Peninsula, north Democratic Republic of the Congo and west Brazil, their
267 carbon sources are significantly increased in both GOSAT and OCO-2 inversions. In east and central
268 Canada, north Europe and west Brazil, there are much stronger carbon sources in OCO-2 inversion.



269

270 **Figure 3.** Distributions of annual land and ocean carbon fluxes a) priori flux and posteriori fluxes
271 based on (b) OCO-2 and (c) GOSAT data ($\text{gC m}^{-2}\text{yr}^{-1}$)

272

273 To better investigate the differences between GOSAT and OCO-2 inversions as well as their



274 differences with the prior fluxes, we aggregate the prior and inferred land fluxes into 11 TRANSCOM
275 land regions (ref.??). Figure 4 shows aggregated annual land surface fluxes from the prior, GOSAT
276 and OCO-2 inversions for the 11 land regions. For comparison purposes, the optimized surface fluxes
277 in CT2016 are also aggregated and shown in Figure 4.

278 **Clearly,** ~~in most regions, the land sinks inverted based on GOSAT data are stronger than those~~
279 ~~inferred from OCO-2 data. In Northern Temperate and Southern Temperate Lands (i.e., North Amer-~~
280 ~~ica Temperate, Eurasian Temperate, Europe, South America Temperate, South Africa and Australia),~~
281 ~~except for Eurasian Temperate and South Africa, the inferred land sinks using GOSAT XCO₂ are~~
282 ~~much stronger than those optimized using OCO-2 data. For example, in North America Temperate,~~
283 ~~the carbon sink of GOSAT experiment (-0.5 Pg C yr⁻¹) is about twice that of the OCO-2 inversions (-~~
284 ~~0.27 Pg C yr⁻¹); and in South America Temperate, the estimated land sink based on GOSAT data (-~~
285 ~~0.47 Pg C yr⁻¹) is about 4 times as large as the OCO-2 inversions (-0.12 Pg C yr⁻¹). For the total~~
286 ~~Temperate Land, the optimized land sinks based on GOSAT and OCO-2 XCO₂ retrievals are -2.95~~
287 ~~and -2.59 Pg C yr⁻¹, respectively (Table 2). In the tropics (i.e., South America Tropical, North Africa,~~
288 ~~and Tropical Asia), except for North Africa, the carbon sinks inferred from GOSAT data are also~~
289 ~~larger than those estimated using OCO-2 data. In Tropical Asia, the estimated land sink based on~~
290 ~~GOSAT data (-0.28 Pg C yr⁻¹) is about 2 times of the OCO-2 inversions (-0.13 Pg C yr⁻¹); in South~~
291 ~~America Tropical, the OCO-2 inversion result is a carbon source of 0.19 PgC yr⁻¹, while GOSAT~~
292 ~~inversion gives a weak sink of -0.05 Pg C yr⁻¹. The total carbon sinks in tropical land inverted from~~
293 ~~GOSAT and OCO-2 data are -0.36 and -0.20 Pg C yr⁻¹, respectively. In Northern Boreal Land, in-~~
294 ~~cluding North America Boreal and Eurasian Boreal, the total carbon sinks inverted with GOSAT (-~~
295 ~~0.18 Pg C yr⁻¹) and OCO-2 (-0.16 Pg C yr⁻¹) data are comparable. However, the two XCO₂ data have~~
296 ~~opposite performances in these two areas, namely in Eurasian Boreal, the inverted land sink with~~
297 ~~GOSAT is stronger than that with OCO-2; while in North America Boreal, it is the opposite.~~



298 ~~For different continents (Table 2), in Asia and Australia, their carbon sinks inverted from GO-~~
299 ~~SAT and OCO-2 data are comparable. In North America, South America and Europe, the land sinks~~
300 ~~in GOSAT inversion are much stronger than those in OCO-2 inversion. Especially in South America,~~
301 ~~the GOSAT inversion result is a strong carbon sink ($-0.51 \text{ Pg C yr}^{-1}$), while in OCO-2 inversion, it is~~
302 ~~a weak carbon source ($0.06 \text{ Pg C yr}^{-1}$). Conversely, in Africa, the land sink estimated with GOSAT~~
303 ~~data is much weaker than those from OCO-2 data, the former ($-0.59 \text{ Pg C yr}^{-1}$) being only about the~~
304 ~~half of the latter ($-1.13 \text{ Pg C yr}^{-1}$).~~

305 ~~Compared with the prior fluxes, basically, the inferred land fluxes in Northern Temperate re-~~
306 ~~gions have largest changes, followed by those in Tropical regions and Southern Temperate lands,~~
307 ~~while in boreal regions, the changes are weakest. Basically, in temperate regions, the inferred land~~
308 ~~sinks are significantly increased, while those in tropical regions are decreased. In boreal regions, the~~
309 ~~changes using two XCO₂ data are not consistent. As shown in Table 3, in Northern Temperate Land,~~
310 ~~the increases of carbon sinks constrained by OCO-2 and GOSAT reach to 1.03 and $1.33 \text{ Pg C yr}^{-1}$,~~
311 ~~respectively, while in Tropical Land, the enhancements of carbon sources are 0.82 and $0.66 \text{ Pg C yr}^{-1}$,~~
312 ~~respectively, whereas in Northern Boreal Land, the changes caused by the two XCO₂ data are only~~
313 ~~0.005 and $-0.015 \text{ Pg C yr}^{-1}$. For different TRANSCOM regions and different XCO₂ used, the changes~~
314 ~~of carbon fluxes have large differences. When using GOSAT data, Europe has the largest change in~~
315 ~~the carbon flux ($-0.63 \text{ Pg C yr}^{-1}$), followed by South America Temperate ($-0.50 \text{ Pg C yr}^{-1}$) and North~~
316 ~~America Temperate ($-0.41 \text{ Pg C yr}^{-1}$); when using OCO-2 data, the largest carbon sink changes are in~~
317 ~~South America Tropical ($0.46 \text{ Pg C yr}^{-1}$) and Eurasian Temperate ($-0.46 \text{ Pg C yr}^{-1}$), followed by Eu-~~
318 ~~rope ($-0.39 \text{ Pg C yr}^{-1}$). Since the same setup used in these two inversions and the same algorithm~~
319 ~~adopted for retrieving XCO₂ from GOSAT and OCO-2 measurements, the different impacts of XCO₂~~
320 ~~data on land sinks may be related to the spatial coverage and the amount of data in these two XCO₂~~
321 ~~datasets. As shown in Figure 1, in different latitude zones, the spatial coverage and the data amount~~
322 ~~of GOSAT and OCO-2 have large differences. Statistics show that basically, the amount of data is~~



323 largest in northern temperate land, followed by southern temperate land and tropical land, and least
324 in northern boreal regions, corresponding to the magnitude of changes of carbon fluxes in these zones.
325 For one specific zone, the different impacts of these two XCO₂ datasets may be also related to their
326 data amount. For example, in northern temperate land, GOSAT has more XCO₂ data than OCO-2.
327 Accordingly, the change of carbon flux caused by GOSAT is larger than that caused by OCO-2. Con-
328 versely, in Tropical Land, OCO-2 has more data than GOSAT, and as shown before it has more sig-
329 nificant impact on the land sink. This relationship could also be found in each TRANSCOM region.
330 Figure 5 gives a relationship between the XCO₂ data amount ratios of GOSAT to OCO-2 and the land
331 sinks absolute change ratios caused by GOSAT to OCO-2 for 11 TRANSCOM land regions. Obvi-
332 ously, except for North and South Africa, there is a significant linear correlation (R=0.95) between
333 these two ratios, suggesting that the more XCO₂ data, the more carbon flux is changed. In North
334 Africa, we find that OCO-2 has better spatial coverage and more data than GOSAT, as shown in
335 Figure 1, although the differences mainly occur in the Sahara where the carbon flux is very weak, but
336 near the equatorial region where the carbon flux is large, OCO-2 still has more data than GOSAT; in
337 southern Africa, both XCO₂ have good spatial coverage, the amount of GOSAT data is about 1.5
338 times that of OCO-2, but the changes in the carbon flux caused by GOSAT is about 10 times that of
339 OCO-2. This indicates that in addition to the spatial coverage and the amount of data, the instrument
340 characteristics such as sensor accuracy and spatial resolution may also have impact on the inversion
341 results.

342 Compared with the CT2016 results, in temperate regions, except for Australia and Europe, the
343 carbon sinks estimated from the two XCO₂ datasets in this study are basically comparable with those
344 inferred based on surface observations in ~~CT2016~~. In Australia and Europe, the inverted carbon sinks
345 with XCO₂ data in this study are both much stronger than CT2016. Especially in Europe, the CT2016
346 estimate is a significant source of 0.26 Pg C, whereas our inversions suggest a strong carbon sink
347 ranging between -0.40 and -0.63 Pg C yr⁻¹. Although previous studies (Basu et al., 2013; Chevallier



348 et al., 2014; Deng et al., 2014; Houweling et al., 2015) also showed enhanced carbon uptake in Europe
349 using GOSAT data, but until now, the strong Europe uptake as inferred from satellite data is still in
350 intense debate (Reuter et al., 2014; Feng et al., 2016; Reuter et al., 2017). Examination of the seasonal
351 variation of the inverted fluxes in Europe shows that during the growing season, both CT2016 and
352 our inversions estimate similar carbon uptake, whereas in the non-growing season, CT2016 produces
353 more carbon release than our inversions. Since there are few satellite measurements in Europe during
354 the dormant season, the carbon release by respiration might not be well constrained by satellite data
355 but close to the prior value.

356 In boreal regions, the inverted land sinks of CT2016 are significantly stronger than those in this
357 study, especially in the Eurasian Boreal, where the carbon uptake estimated by CT2016 is almost 1
358 Pg C yr⁻¹ larger than our estimates. One explanation for the large sink in CT2016 in this area is that
359 there is a mutual compensation for carbon sinks between Europe and Eurasian Boreal because of the
360 large differences in the amount of observations between these two areas. Kim et al. (2017) found that
361 with the addition of Siberian in-situ measurements to their inversion system, the carbon uptake in
362 Europe was enhanced while it decreased in the boreal Eurasian. Saeki et al. (2013) also reported that
363 more CO₂ observations over Siberian used in the inversion system would weaken the summer carbon
364 uptake in this area. These studies indicate that for CT2016, the carbon sink in Europe may be under-
365 estimated, while in boreal Eurasian, it may be significantly overestimated. Since there are only very
366 few XCO₂ observations from both GOSAT and OCO-2 in this area, our estimates are very close to
367 the prior and much weaker than those found by Saeki et al. (2013) and Kim et al. (2017), indicating
368 that the land sink in the Eurasian Boreal is underestimated in this study. Combined the land sinks of
369 Europe and Eurasian Boreal, the inverted land sinks of GOSAT (-0.86 Pg C yr⁻¹) is comparable with
370 CT2016 (-0.92 Pg C yr⁻¹), indicating that the land sink in Europe inferred from GOSAT may be also
371 overestimated to a certain extent.

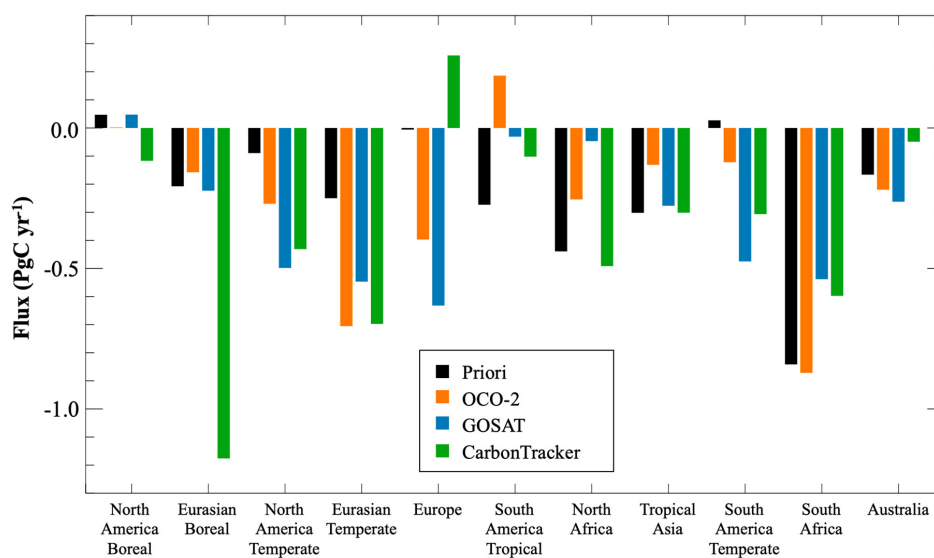
372 In the tropical regions, the inverted land sinks of CT2016 are also all much stronger than our



373 estimates, but the differences between the inverted and the prior fluxes in CT2016 are significantly
374 smaller than those in this study, mainly because of the lack of surface CO₂ observations in tropical
375 areas, especially in Tropical Asia.

376 For different continents (Table 2), the largest difference between this study and CT2016 is found
377 in Asia. Using an ensemble of seven atmospheric inverse systems, Thompson et al. (2016) reported
378 that the Asian land biosphere CO₂ flux (including land-use change and fires) was a net sink of -0.46
379 (-0.70~0.24) Pg C yr⁻¹ (median and range) for 1996–2012. The land biosphere CO₂ fluxes (also in-
380 cluding biomass burning emissions) estimated based on OCO-2 and GOSAT in this study are -0.37
381 and -0.42 Pg C yr⁻¹, respectively, which are comparable with the result of Thompson et al. (2016).

382



383

384 **Figure 4.** Aggregated annual land fluxes of the 11 TRANSKOM land regions

385

386

387

388


 389 **Table 2.** The priori and posteriori fluxes in six continents and boreal, temperate and tropical lands

Regions	Prior	OCO-2	GOSAT	CT2016
North America	-0.04	-0.27	-0.45	-0.55
South America	-0.25	0.06	-0.51	-0.41
Europe	-0.01	-0.40	-0.63	0.26
Asia	-0.76	-0.99	-1.05	-2.18
Africa	-1.28	-1.13	-0.59	-1.09
Australia	-0.17	-0.22	-0.26	-0.05
Northern Boreal Land	-0.16	-0.16	-0.18	-1.29
Northern Temperate Land	-0.35	-1.37	-1.68	-0.87
Tropical Land	-1.01	-0.20	-0.36	-0.90
Southern Temperate Land	-0.98	-1.21	-1.28	-0.95

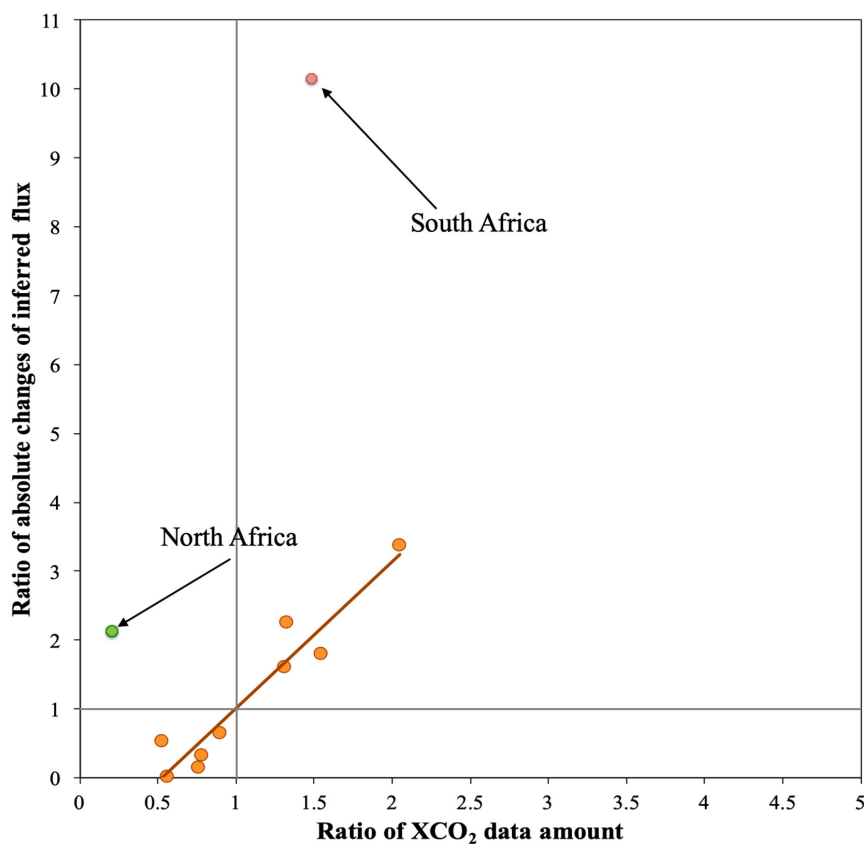
390

 391 **Table 3.** Differences between the inferred and the prior carbon fluxes, and the data amount of XCO₂
 392 in different regions

Region	Differences (Pg C yr ⁻¹)		XCO ₂ data amount	
	OCO-2	GOSAT	OCO-2	GOSAT
North America Boreal	-0.05	0.00	1143	639
North America Temperate	-0.18	-0.41	2390	3163
South America Tropical	0.46	0.24	800	421
South America Temperate	-0.15	-0.50	1711	3500
North Africa	0.19	0.39	3208	674
South Africa	-0.03	0.30	2057	3060
Eurasian Boreal	0.05	-0.02	1714	1339
Eurasian Temperate	-0.46	-0.30	5323	4782
Tropical Asia	0.17	0.03	726	550
Australia	-0.05	-0.10	2011	3110
Europe	-0.39	-0.63	1604	2106
Global land	-0.44	-0.98	22687	23344
Northern Boreal Land	0.005	-0.02	2857	1978
Northern Temperate Land	-1.03	-1.33	9317	10051
Tropical Land	0.82	0.66	4734	1645
Southern Temperate Land	-0.23	-0.30	5779	9670



393



394

395 **Figure 5.** Scatter plot for the ratio of GOSAT to OCO-2 XCO₂ data amount versus the ratio of abso-
396 lute changes of the land sinks caused by GOSAT to OCO-2 in the 11 TRANSCOM land regions
397

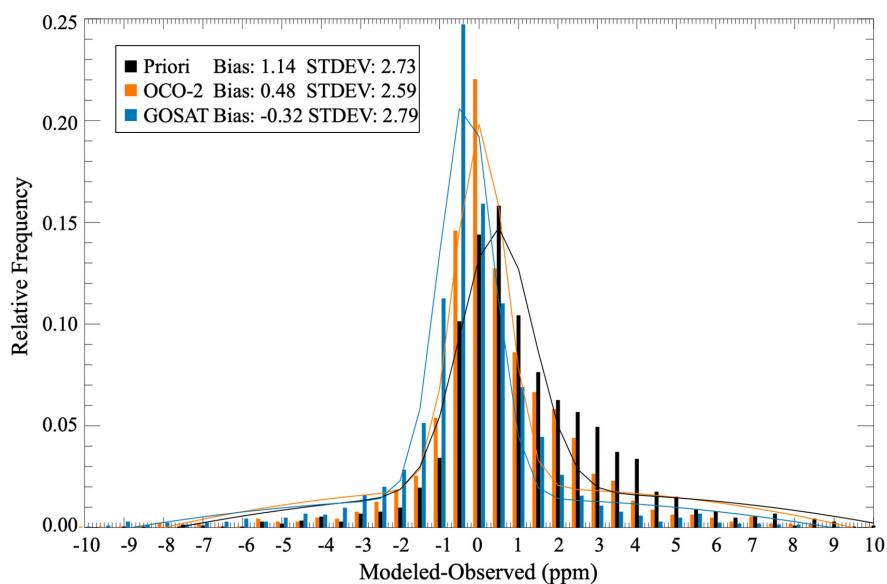
398 4.3 Evaluation for the inversion results

399 4.3.1 Flask observations

400 We use flask observations from 47 surface sites (Figure 2) to evaluate the posterior fluxes. The
401 GEOS-Chem model is driven with the prior flux and the two posterior fluxes to obtain the prior and
402 posterior CO₂ mixing ratios. The simulated CO₂ mixing ratios are sampled at each observation site
403 and within half an hour of observation time. Figure 6 shows a summary of comparisons of the simu-
404 lated CO₂ mixing ratio against the flask measurements. The mean difference between the prior CO₂
405 mixing ratio and the flask measurements is 1.14 ppm, with a standard deviation of 2.73 ppm. Using

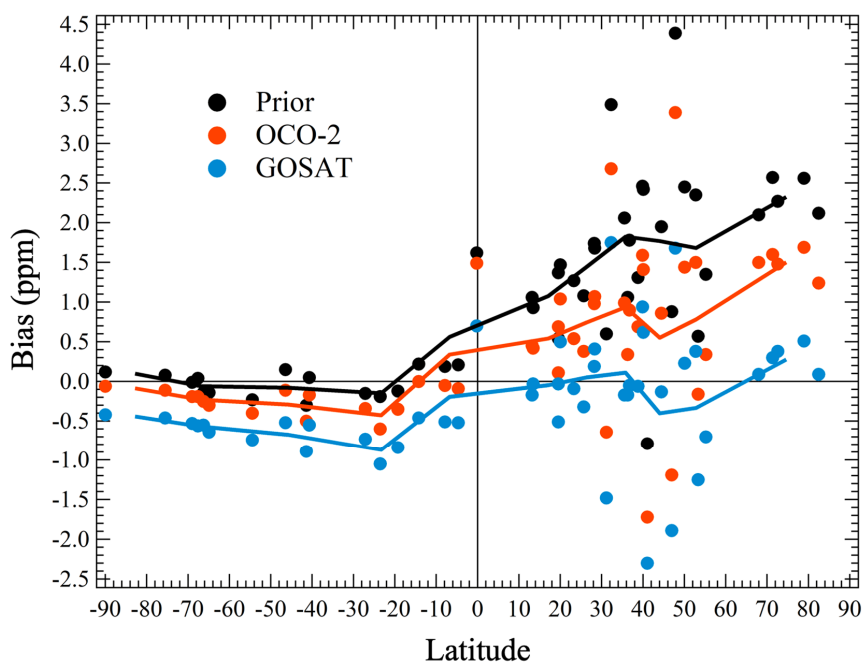


406 posterior fluxes inferred from GOSAT and OCO-2 data, the mean differences between the posterior
407 CO₂ mixing ratio and flask measurements are reduced to -0.32 and 0.48 ppm, with a standard devia-
408 tion of 2.59 and 2.79 ppm, respectively. It is noted that the mean difference in the posterior CO₂
409 mixing ratio between GOSAT and OCO-2 inversions at 47 observation sites is 0.8 ppm, much larger
410 than the 0.26 ppm (0.56 Pg C/2.12 Pg C/ppm=0.26 ppm) difference between their global net flux
411 estimates, indicating the relatively large difference in posterior flux between these two inversions at
412 the regional scale. Figure 7 shows the biases at each observation site in different latitudes. It could be
413 found that the biases between the simulations and the observations in the northern hemisphere are
414 significantly larger than those in southern hemisphere since the carbon flux distribution of the north-
415 ern hemisphere is more complex than that of the southern hemisphere. When the prior flux is used,
416 almost all sites in the northern hemisphere have significant positive deviations, with an average of
417 1.7 ppm, while in the southern hemisphere, the deviations are very small, with an average bias of
418 only 0.08 ppm; when using the posterior flux of OCO-2, the deviations in most northern hemisphere
419 sites are significantly reduced, with the average deviation falling to half the original, to 0.85 ppm,
420 while in the southern hemisphere, at most sites, the biases increase by variable amounts, with a mean
421 of -0.13 ppm; when using the posterior flux of GOSAT, the deviations are further reduced to -0.04
422 ppm in the northern hemisphere but further increased to -0.55 ppm in the southern hemisphere. These
423 suggest that GOSAT and OCO-2 data can effectively improve the carbon fluxes estimate in the north-
424 ern hemisphere, but overestimate the land sinks in the southern hemisphere, especially for GOSAT.
425



426

427 **Figure 6.** Statistical distribution of the modeled and observed mismatch errors in 47 surface flask
428 sites



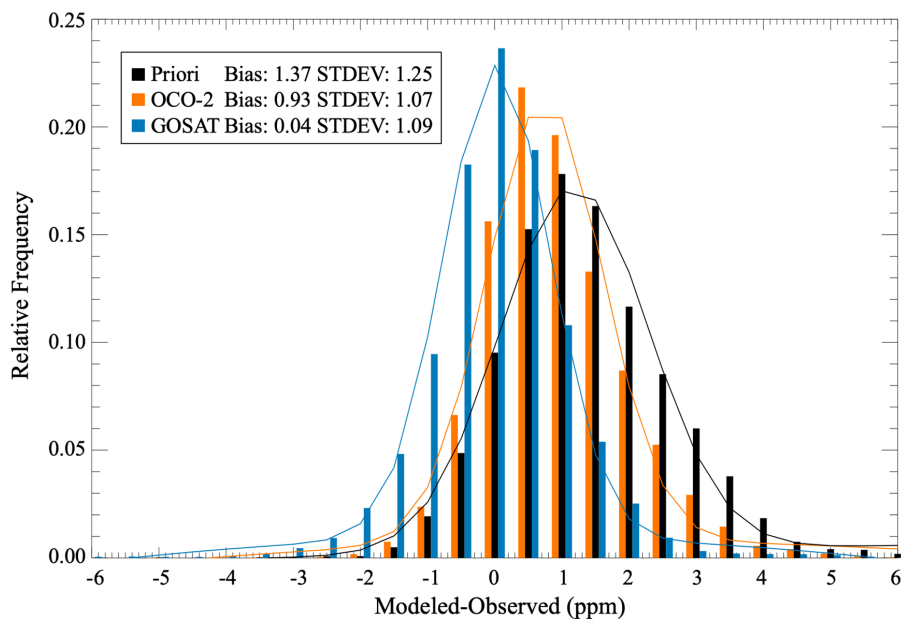
429

430 **Figure 7.** Biases of the simulated CO₂ mixing ratios against the flask measurements in different lat-
431 itudes (positive/negative biases represent modeled concentration being greater/less than the ob-
432 served)



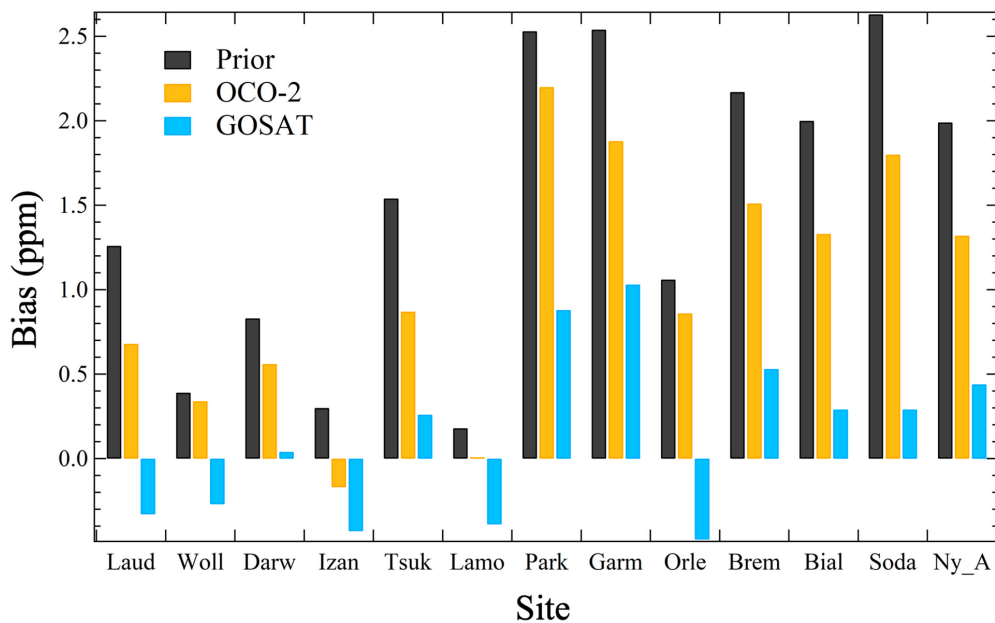
433 4.3.2 TCCON observations

434 We also use ground XCO₂ observations from 13 TCCON sites (Figure 2) to evaluate our inver-
435 sion results. The simulated CO₂ concentrations at 47 vertical levels are mapped into 71 TCCON
436 levels. Following the approach of Wunch et al. (2011), using prior profiles and the averaging kernel
437 from the TCCON dataset, we calculated the modeled XCO₂ values at 13 TCCON sites. Figure 6
438 shows the comparison of modeled XCO₂ with TCCON observations. The mean difference between
439 prior XCO₂ and TCCON observations is 1.37 ppm, with a standard deviation of 1.25 ppm. Through
440 OCO-2 inversion, the mean difference between modeled and observed XCO₂ is slightly reduced to
441 0.93 ppm, with a standard deviation of 1.07 ppm, and through GOSAT inversion, the mean differ-
442 ence between modeled and observed XCO₂ is significantly reduced to 0.04 ppm with a standard de-
443 viation of 1.09 ppm. Figure 9 shows the bias at each TCCON site. Obviously, the biases at all
444 TCCON sites are positive when using the prior fluxes, ranging between 0.3 and 2.6 ppm. The bi-
445 ases at the sites in the northern temperate and boreal areas are all above 1.5 ppm except for the La-
446 mont site. After using the posterior fluxes of OCO-2, the biases of all sites are reduced by 30%. Af-
447 ter using the posteriori fluxes of GOSAT, the biases are significantly reduced, ranging between -
448 0.48 and 1.03 ppm. For two of the three TCCON sites in the southern hemisphere, the biases are
449 changed to negative values when using the posteriori fluxes from GOSAT data, further indicating
450 the overestimation of carbon sinks by GOSAT data in the southern hemisphere.



451

452 **Figure 8.** Statistical distributions of modeled and observed mismatch errors at 13 TCCON sites



453

454 **Figure 9.** The biases between the modeled and observed XCO₂ at the 13 TCCON sites

455



456 5. Summary and Conclusions

457 In this study, we use both GOSAT and OCO-2 XCO₂ retrievals to constrain terrestrial ecosys-
458 tem carbon fluxes from Oct 1, 2014 to Dec 31, 2015, using a 4D-Var system within the GEOS-Chem
459 adjoint model. The posterior carbon fluxes estimated from GOSAT and OCO-2 data at both global
460 and regional scales during Jan 1 to Dec 31, 2015 are shown and discussed. Surface CO₂ mixing ratios
461 from 47 surface flask sites and XCO₂ observations from 13 TCCON sites are used to evaluate the
462 inversions of carbon fluxes using GOSAT and OCO-2 data.

463 Globally, the land net flux (including fossil fuel and biomass burning emissions) inferred from
464 GOSAT and OCO-2 XCO₂ retrievals are larger than the prior value, and lower than the estimate of
465 CT2016, but much closer to the estimate of GCP 2017. The terrestrial ecosystem carbon sink (ex-
466 cluding biomass burning emissions) estimated from GOSAT data is stronger than that inferred from
467 OCO-2 data, and the annual atmospheric CO₂ growth rate (global net flux) estimated based on GO-
468 SAT data is more consistent with the GCP estimate than that based on OCO-2. Regionally, in most
469 regions, the land sinks inverted based on GOSAT data are also stronger than those inferred from
470 OCO-2 data. Compared with the prior fluxes, ~~basically~~, the inferred land sinks are significantly in-
471 creased in northern and southern temperate regions, and decreased in tropical regions. In addition,
472 the inferred carbon fluxes have the largest changes in Northern Temperate regions, followed by Trop-
473 ical and Southern Temperate regions, and the weakest in boreal regions. The different impact of XCO₂
474 on the carbon fluxes in different regions are mainly related to the spatial coverage and the amount of
475 XCO₂ data. Generally, a larger amount of XCO₂ data in a region is corresponding to a larger change
476 in the inverted carbon flux in the same region. Compared with the CT2016 results, the carbon sinks
477 optimized using XCO₂ in this study are comparable with CT2016 in most temperate regions, but
478 much weaker than CT2016 in the boreal and tropical regions.

479 Evaluations of the inversions using CO₂ concentrations from flask and TCCON measurements
480 showed that both posterior carbon fluxes of OCO-2 and GOSAT could significantly improve the



481 modeling of atmospheric CO₂ concentrations, and both the simulated surface CO₂ mixing ratio and
482 XCO₂ concentrations with GOSAT posterior fluxes are much closer to the observations than those
483 with OCO-2. Generally, in the northern hemisphere, the deviations are significantly reduced, while
484 in the southern hemisphere, the biases are elevated to a certain extent. These suggest that GOSAT and
485 OCO-2 data can effectively improve the carbon fluxes estimate in the northern hemisphere, while in
486 the southern hemisphere and some northern temperate regions, the optimized carbon sinks may be
487 overestimated.

488 **Author contributions**

489 FJ and HW designed the research, HW conducted inverse modeling, HW and FJ conducted data anal-
490 ysis and wrote the paper, JW, WJ and JC participated in the discussion of the results and provided
491 input on the paper for revision before submission.

492 **Competing interests**

493 The authors declare that they have no conflict of interest.

494 **Acknowledgements**

495 This work is supported by the National Key R&D Program of China (Grant No: 2016YFA0600204), National
496 Natural Science Foundation of China (Grant No: 41571452), and the Fundamental Research Funds for the
497 Central Universities (Grant No: 090414380021).

498

499 **References**

- 500 Andres, R. J., Gregg, J. S., Losey, L., Marland, G. and Boden, T. A.: Monthly, global emissions of carbon
501 dioxide from fossil fuel consumption. *Tellus B*, 63(3), 309–327, [https://doi.org/10.1111/j.1600-](https://doi.org/10.1111/j.1600-0889.2011.00530.x)
502 [0889.2011.00530.x](https://doi.org/10.1111/j.1600-0889.2011.00530.x), 2011.
- 503 Baker, D. F., Bösch, H., Doney, S. C., O'Brien, D., and Schimel, D. S.: Carbon source/sink information pro-
504 vided by column CO₂ measurements from the Orbiting Carbon Observatory, *Atmos. Chem. Phys.*, 10,
505 4145–4165, <https://doi.org/10.5194/acp-10-4145-2010>, 2010.
- 506 Basu, S., Guerlet, S., Butz, A., Houweling, S., Hasekamp, O., Aben, I., Krummel, P., Steele, P., Langenfelds,
507 R., Torn, M., Biraud, S., Stephens, B., Andrews, A., and Worthy, D.: Global CO₂ fluxes estimated from
508 GOSAT retrievals of total column CO₂, *Atmos. Chem. Phys.*, 13, 8695–8717,
509 <https://doi.org/10.5194/acp-13-8695-2013>, 2013.



- 510 Basu, S., Krol, M., Butz, A., Clerbaux, C., Sawa, Y., Machida, T., Matsueda, H., Frankenberg, C., Hasekamp,
511 O. P., and Aben, I.: The seasonal variation of the CO₂ flux over Tropical Asia estimated from GOSAT,
512 CONTRAIL, and IASI, *Geophys. Res. Lett.*, 41, 1809–1815, <https://doi.org/10.1002/2013GL059105>,
513 2014.
- 514 Blumenstock, T., Hase, F., Schneider, M., García, O.E., and Sepúlveda, E.: TCCON data from Izana, Tene-
515 rife, Spain, Release GGG2014R1. TCCON data archive, hosted by CaltechDATA, California Institute of
516 Technology, Pasadena, CA, U.S.A. <https://doi.org/10.14291/tcon.ggg2014.izana01.R1>, 2017.
- 517 Byrd, R. H., Nocedal, J. and Schnabel, R. B.: Representations of Quasi-Newton Matrices and their use in
518 Limited Memory Methods. *Math Program.* 63(4), 129–156. <https://doi.org/10.1007/BF01582063>, 1994.
- 519 Chatterjee, A., Gierach, M. M., Sutton, A. J., Feely, R. A., Crisp, D., Eldering, A., Gunson, M. R., O'Dell, C.
520 W., Stephens, B. B., and Schimel, D. S.: Influence of El Niño on atmospheric CO₂ over the tropical Pa-
521 cific Ocean: Find- ings from NASA's OCO-2 mission, *Science*, 358, eaam5776,
522 <https://doi.org/10.1126/science.aam5776>, 2017.
- 523 Chevallier, F., Bron, F.-M., and Rayner, P. J.: Contribution of the Orbiting Carbon Observatory to the estima-
524 tion of CO₂ sources and sinks: Theoretical study in a variational data assimilation framework, *J. Geophys.*
525 *Res.-Atmos.*, 112, d09307, <https://doi.org/10.1029/2006JD007375>, 2007.
- 526 Chevallier, F., Feng, L., Bösch, H., Palmer, P. I., and Rayner, P. J.: On the impact of transport model errors
527 for the estimation of CO₂ surface fluxes from GOSAT observations, *Geophys. Res. Lett.*, 37, L21803,
528 <https://doi.org/10.1029/2010GL044652>, 2010.
- 529 Chevallier, F., Palmer, P. I., Feng, L., Boesch, H., O'Dell, C. W., and Bousquet, P.: Toward robust and con-
530 sistent regional CO₂ flux estimates from in situ and spaceborne measurements of atmospheric CO₂, *Ge-*
531 *ophys. Res. Lett.*, 41, 1065–1070, <https://doi.org/10.1002/2013GL058772>, 2014.
- 532 Corbett, J. J., and Koehler, H. W.: Updated emissions from ocean shipping, *J. Geophys. Res.*, 108, 4650,
533 <https://doi.org/10.1029/2003JD003751>, D20, 2003.
- 534 Conway, T. J., Tans, P. P., Waterman, L. S., Thoning, K. W., Kitzis, D. R., Masarie, K. A., and Zhang, N.: Ev-
535 idence for interannual variability of the carbon cycle from the National Oceanic and Atmospheric Admin-
536 istration/Climate Monitoring and Diagnostics Laboratory Global Air Sampling Network, *J. Geophys.*
537 *Res.*, 99, 22831–22855, <https://doi.org/10.1029/94JD01951>, 1994.
- 538 Crisp, D., Pollock, H. R., Rosenberg, R., Chapsky, L., Lee, R. A. M., Oyafuso, F. A., Frankenberg, C.,
539 O'Dell, C. W., Bruegge, C. J., Doran, G. B., Eldering, A., Fisher, B. M., Fu, D., Gunson, M. R., Man-
540 drake, L., Osterman, G. B., Schwandner, F. M., Sun, K., Taylor, T. E., Wennberg, P. O., and Wunch, D.:
541 The on-orbit performance of the Orbiting Carbon Observatory-2 (OCO-2) instrument and its radiometri-
542 cally calibrated products, *Atmos. Meas. Tech.*, 10, 59–81, <https://doi.org/10.5194/amt-10-59-2017>, 2017.
- 543 Deng, F. and Chen, J. M.: Recent global CO₂ flux inferred from atmospheric CO₂ observations and its re-
544 gional analyses, *Biogeo- sciences*, 8, 3263–3281, <https://doi.org/10.5194/bg-8-3263-2011>, 2011.
- 545 Deng, F., Jones, D. B. A., Henze, D. K., Bousserez, N., Bowman, K. W., Fisher, J. B., Nassar, R., O'Dell, C.,
546 Wunch, D., Wennberg, P. O., Kort, E. A., Wofsy, S. C., Blumenstock, T., Deutscher, N. M., Griffith, D. W.
547 T., Hase, F., Heikkinen, P., Sherlock, V., Strong, K., Sussmann, R., and Warneke, T.: Inferring regional
548 sources and sinks of atmospheric CO₂ from GOSAT XCO₂ data, *Atmos. Chem. Phys.*, 14, 3703–3727,
549 <https://doi.org/10.5194/acp-14-3703-2014>, 2014.
- 550 Deng, F., Jones, D. B. A., O'Dell, C. W., Nassar, R., and Parazoo, N. C.: Combining GOSAT XCO₂ observa-
551 tions over land and ocean to improve regional CO₂ flux estimates, *J. Geophys. Res. Atmos.*, 121, 1896–
552 1913, <https://doi.org/10.1002/2015JD024157>, 2016.
- 553 Deutscher, N., Notholt, J., Messerschmidt, J., Weinzierl, C., Warneke, T., Petri, C., Grupe, P., and Katrynski,
554 K.: TCCON data from Bialystok, Poland, Release GGG2014R1. TCCON data archive, hosted by Cal-
555 techDATA, California Institute of Technology, Pasadena, CA, U.S.A.
556 <http://doi.org/10.14291/tcon.ggg2014.bialystok01.R1/1183984>, 2017.
- 557 Eldering, A., Boland, S., Solish, B., Crisp, D., Kahn, P., and Gunson, M.: High precision atmospheric CO₂



- 558 measurements from space: The design and implementation of OCO-2, in: 2012 IEEE Aerospace Confer-
559 ence, 1–10, <https://doi.org/10.1109/AERO.2012.6187176>, 2012.
- 560 Eldering, A., O'Dell, C. W., Wennberg, P. O., Crisp, D., Gunson, M. R., Viatte, C., Avis, C., Braverman, A.,
561 Castano, R., Chang, A., Chapsky, L., Cheng, C., Connor, B., Dang, L., Doran, G., Fisher, B., Frankenberg,
562 C., Fu, D., Granat, R., Hobbs, J., Lee, R. A. M., Mandrake, L., McDuffie, J., Miller, C. E., Myers, V., Natraj,
563 V., O'Brien, D., Osterman, G. B., Oyafuso, F., Payne, V. H., Pollock, H. R., Polonsky, I., Roehl, C. M.,
564 Rosenberg, R., Schwandner, F., Smyth, M., Tang, V., Taylor, T. E., To, C., Wunch, D., and Yoshimizu, J.:
565 The Orbiting Carbon Observatory-2: first 18 months of science data products, *Atmos. Meas. Tech.*, 10,
566 549–563, <https://doi.org/10.5194/amt-10-549-2017>, 2017a.
- 567 Eldering, A., Wennberg, P. O., Crisp, D., Schimel, D. S., Gunson, M. R., Chatterjee, A., Liu, J., Schwand-
568 ner, F. M., Sun, Y., O'Dell, C. W., Frankenberg, C., Taylor, T., Fisher, B., Osterman, G. B., Wunch, D.,
569 Hakkarainen, J., Tamminen, J., and Weir, B.: The Orbiting Carbon Observatory-2 early science investiga-
570 tions of regional carbon dioxide fluxes, *Science*, 358, eaam5745, <https://doi.org/10.1126/sci->
571 [ence.aam5745](https://doi.org/10.1126/science.aam5745), 2017b.
- 572 Endresen, Ø., Sørgård, E., Behrens, H. L., Brett, P. O., and Isaksen, I. S. A.: A historical reconstruction of
573 ships' fuel consumption and emissions, *J. Geophys. Res.*, 112, D12301,
574 <https://doi.org/10.1029/2006JD007630>, 2007.
- 575 Feng, L., Palmer, P. I., Parker, R. J., Deutscher, N. M., Feist, D. G., Kivi, R., Morino, I., and Sussmann, R.:
576 Estimates of European uptake of CO₂ inferred from GOSAT XCO₂ retrievals: Sensitivity to measurement
577 bias inside and outside Europe. *Atmos. Chem. Phys.*, 16, 1289–1302, <https://doi.org/10.5194/acp-16->
578 1289-2016, 2016.
- 579 Giglio, L., Randerson, J. T., and van der Werf, G. R.: Analysis of daily, monthly, and annual burned area us-
580 ing the fourth-generation global fire emissions database (GFED4) *J. Geophys. Res. Biogeosci.*, 118, 317–
581 328, <https://doi.org/10.1002/jgrg.20042>, 2013.
- 582 Griffith, D. W. T., Deutscher, N., Velazco, V. A., Wennberg, P. O., Yavin, Y., Keppel Aleks, G.,
583 Washenfelder, R., Toon, G. C., Blavier, J.-F., Murphy, C., Jones, N., Kettlewell, G., Connor,
584 B., Macatangay, R., Roehl, C., Ryzcek, M., Glowacki, J., Culgan, T., and Bryant, G.: TCCON
585 data from Darwin, Australia, Release GGG2014R0. TCCON data archive, hosted by Cal-
586 techDATA, California Institute of Technology, Pasadena, CA, U.S.A.
587 <http://doi.org/10.14291/tcon.ggg2014.darwin01.R0/1149290>, 2017a.
- 588 Griffith, D. W. T., Velazco, V. A., Deutscher, N., Murphy, C., Jones, N., Wilson, S., Macatangay,
589 R., Kettlewell, G., Buchholz, R. R., and Riggensbach, M.: TCCON data from Wollongong,
590 Australia, Release GGG2014R0. TCCON data archive, hosted by CaltechDATA, California
591 Institute of Technology, Pasadena, CA, U.S.A. <https://doi.org/10.14291/tcon.ggg2014.wol->
592 [longong01.R0/1149291](https://doi.org/10.14291/tcon.ggg2014.wollongong01.R0/1149291), 2017b.
- 593 Henze, D. K., Hakami, A. and Seinfeld, J. H.: Development of the adjoint of GEOS-Chem, *Atmos. Chem.*
594 *Phys.*, 7, 2413–2433, 2007.
- 595 Heymann, J., Reuter, M., Buchwitz, M., Schneising, O., Bovensmann, H., Burrows, J. P., Massart, S., Kai-
596 ser, J. W., and Crisp, D.: CO₂ emission of Indonesian fires in 2015 estimated from satellite-derived atmos-
597 pheric CO₂ concentrations, *Geophys. Res. Lett.*, 44, 1537–1544, <https://doi.org/10.1002/2016GL072042>,
598 2017.
- 599 Houweling, S., Breon, F.-M., Aben, I., Rødenbeck, C., Gloor, M., Heimann, M., and Ciais, P.: Inverse mod-
600 eling of CO₂ sources and sinks using satellite data: a synthetic inter-comparison of measurement tech-
601 niques and their performance as a function of space and time, *Atmos. Chem. Phys.*, 4, 523–538,
602 <https://doi.org/10.5194/acp-4-523-2004>, 2004.
- 603 Houweling, S., Aben, I., Breon, F.-M., Chevallier, F., Deutscher, N., Engelen, R., Gerbig, C., Griffith, D.,
604 Hungershofer, K., Macatangay, R., Marshall, J., Notholt, J., Peters, W., and Serrar, S.: The importance of
605 transport model uncertainties for the estimation of CO₂ sources and sinks using satellite measurements,
606 *Atmos. Chem. Phys.*, 10, 9981–9992, <https://doi.org/10.5194/acp-10-9981-2010>, 2010.
- 607



- 608 Houweling, S., Baker, D., Basu, S., Boesch, H., Butz, A., Cheval-
609 L., Ganshin, A., Hasekamp, O., Jones, D., Maksyutov, S., Marshall, J., Oda, T., O'Dell, C. W.,
610 Oshchepkov, S., Palmer, P. I., Peylin, P., Poussi, Z., Reum, F., Takagi, H., Yoshida, Y., and Zhuravlev, R.:
611 An intercomparison of inverse models for estimating sources and sinks of CO₂ using GOSAT measure-
612 ments, *J. Geophys. Res.-Atmos.*, 120, 5253–5266, <https://doi.org/10.1002/2014JD022962>, 2015.
- 613 Hungershofer, K., Breon, F.-M., Peylin, P., Chevallier, F., Rayner, P., Klonecki, A., Houweling, S., and Mar-
614 shall, J.: Evaluation of various observing systems for the global monitoring of CO₂ surface fluxes, *Atmos.*
615 *Chem. Phys.*, 10, 10503–10520, <https://doi.org/10.5194/acp-10-10503-2010>, 2010.
- 616 Jiang, Z., Jones, D. B. A., Kopacz, M., Liu, J., Henze, D. K., and Heald, C.: Quantifying the impact of model
617 errors on top-down estimates of carbon monoxide emissions using satellite observations, *J. Geophys.*
618 *Res.*, 116, D15306, <https://doi.org/10.1029/2010JD015282>, 2011.
- 619 Kim, B. Y., Fleming, G. G., Lee, J. J., Waitz, I. A., Clarke, J.-P., Balasubramanian, S., Malwitz, A., Klima,
620 K., Locke, M., Holsclaw, C. A., Maurice, L. Q., Gupta, M. L.: System for assessing Aviation's Global
621 Emissions (SAGE), Part 1: Model description and inventory results, *Transportation Research Part D:*
622 *Transport and Environment*, 12(5), 325-346, <https://doi.org/10.1016/j.trd.2007.03.007>, 2007.
- 623 Kim, J., Kim, H. M., Cho, C.-H., Boo, K.-O., Jacobson, A. R., Sasakawa, M., Machida, T., Arshinov, M., and
624 Fedoseev, N.: Impact of Siberian observations on the optimization of surface CO₂ flux, *Atmos. Chem.*
625 *Phys.*, 17, 2881-2899, <https://doi.org/10.5194/acp-17-2881-2017>, 2017.
- 626 Kivi, R., Heikkinen, P., and Kyro, E.: TCCON data from Sodankyla, Finland, Release
627 GGG2014R0. TCCON data archive, hosted by CaltechDATA, California Institute of Technol-
628 ogy, Pasadena, CA, U.S.A. <https://doi.org/10.14291/tcon.ggg2014.sodankyla01.R0/1149280>,
629 2017.
- 630 Kopacz, M., Jacob, D. J., Henze, D. K., Heald, C. L., Streets, D. G., and Zhang, Q.: A comparison of analyti-
631 cal and adjoint Bayesian inversion methods for constraining Asian sources of CO using satellite
632 (MOPITT) measurements of CO columns, *J. Geophys. Res.*, 114, D04305,
633 <https://doi.org/10.1029/2007JD009264>, 2009.
- 634 Kopacz, M., Jacob, D. J., Fisher, J. A., Logan, J. A., Zhang, L., Megretskaia, I. A., Yantosca, R. M., Singh, K.,
635 Henze, D. K., Burrows, J. P., Buchwitz, M., Khlystova, I., McMillan, W. W., Gille, J. C., Edwards, D. P.,
636 Eldering, A., Thouret, V., and Nedelec, P.: Global estimates of CO sources with high resolution by adjoint
637 inversion of multiple satellite datasets (MOPITT, AIRS, SCIAMACHY, TES), *Atmos. Chem. Phys.*, 10,
638 855-876, 2010.
- 639 Kuze, A., Suto, H., Nakajima, M., and Hamazaki, T.: Thermal and near infrared sensor for carbon observa-
640 tion Fourier-transform spectrometer on the Greenhouse Gases Observing Satellite for greenhouse gases
641 monitoring. *Appl. Opt.*, 48, 6716, <https://doi.org/10.1364/AO.48.006716>, 2009.
- 642 Le Quéré, C., Andrew, R. M., Friedlingstein, P., Sitch, S., Pongratz, J., Manning, A. C., Korsbakken, J. I.,
643 Peters, G. P., Canadell, J. G., Jackson, R. B., Boden, T. A., Tans, P. P., Andrews, O. D., Arora, V. K., Bak-
644 ker, D. C. E., Barbero, L., Becker, M., Betts, R. A., Bopp, L., Chevallier, F., Chini, L. P., Ciais, P., Cosca,
645 C. E., Cross, J., Currie, K., Gasser, T., Harris, I., Hauck, J., Haverd, V., Houghton, R. A., Hunt, C. W.,
646 Hurtt, G., Ilyina, T., Jain, A. K., Kato, E., Kautz, M., Keeling, R. F., Klein Goldewijk, K., Körtzinger, A.,
647 Landschützer, P., Lefèvre, N., Lenton, A., Lienert, S., Lima, I., Lombardozzi, D., Metzl, N., Millero, F.,
648 Monteiro, P. M. S., Munro, D. R., Nabel, J. E. M. S., Nakaoka, S.-I., Nojiri, Y., Padin, X. A., Pregon, A.,
649 Pfeil, B., Pierrot, D., Poulter, B., Rehder, G., Reimer, J., Rödenbeck, C., Schwinger, J., Séférian, R.,
650 Skjelvan, I., Stocker, B. D., Tian, H., Tilbrook, B., Tubiello, F. N., van der Laan-Luijckx, I. T., van der
651 Werf, G. R., van Heuven, S., Viovy, N., Vuichard, N., Walker, A. P., Watson, A. J., Wiltshire, A. J.,
652 Zaehle, S., and Zhu, D.: Global Carbon Budget 2017, *Earth Syst. Sci. Data*, 10, 405-448,
653 <https://doi.org/10.5194/essd-10-405-2018>, 2018.
- 654 Liu, J., Bowman, K. W., Lee, M., Henze, D. K., Bousserez, N., Brix, H., Collatz, G. J., Menemenlis, D., Ott,
655 L., Pawson, S., Jones, D., and Nassar, R.: Carbon monitoring system flux estimation and attribution: im-
656 pact of ACOS-GOSAT XCO₂ sampling on the inference of terrestrial biospheric sources and sinks, *Tellus*
657 *B*, 66, 22486, <https://doi.org/10.3402/tellusb.v66.22486>, 2014.



- 658 Liu, J., Bowman, K. W., Schimel, D. S., Parazoo, N. C., Jiang, Z., Lee, M., Bloom, A. A., Wunch, D., Frank-
659 enberg, C., Sun, Y., O'Dell, C. W., Gurney, K. R., Menemenlis, D., Gierach, M., Crisp, D., and Eldering,
660 A.: Contrasting carbon cycle responses of the tropical continents to the 2015–2016 El Niño, *Science*, 358,
661 eaam5690, <https://doi.org/10.1126/science.aam5690>, 2017.
- 662 Maksyutov, S., Takagi, H., Valsala, V. K., Saito, M., Oda, T., Sasaki, T., Belikov, D. A., Saito, R., Ito, A., Yo-
663 shida, Y., Morino, I., Uchino, O., Andres, R. J., and Yokota, T.: Regional CO₂ flux estimates for 2009–
664 2010 based on GOSAT and ground- based CO₂ observations, *Atmos. Chem. Phys.*, 13, 9351–9373,
665 <https://doi.org/10.5194/acp-13-9351-2013>, 2013.
- 666 Miller, C. E., Crisp, D., DeCola, P. L., Olsen, S. C., Randerson, J. T., Michalak, A. M., Alkhaled, A., Rayner,
667 P., Jacob, D. J., Suntharalingam, P., Jones, D. B. A., Denning, A. S., Nicholls, M. E., Doney, S. C., Paw-
668 son, S., Boesch, H., Connor, B. J., Fung, I. Y., O'Brien, D., Salawitch, R. J., Sander, S. P., Sen, B., Tans,
669 P., Toon, G. C., Wennberg, P. O., Wofsy, S. C., Yung, Y. L., and Law, R. M.: Precision requirements for
670 space-based XCO₂ data, *J. Geophys. Res.*, 112, D10314, <https://doi.org/10.1029/2006JD007659>, 2007.
- 671 Miller, S. M., Michalak, A. M., Yadav, V., and Tadić, J. M.: Characterizing biospheric carbon balance using
672 CO₂ observations from the OCO-2 satellite, *Atmos. Chem. Phys.*, 18, 6785–6799,
673 <https://doi.org/10.5194/acp-18-6785-2018>, 2018.
- 674 Morino, I., Matsuzaki, T., and Shishime, A.: TCCON data from Tsukuba, Ibaraki, Japan, 125HR,
675 Release GGG2014R2. TCCON data archive, hosted by CaltechDATA, California Institute of
676 Technology, Pasadena, CA, U.S.A. <http://doi.org/10.14291/tcon.ggg2014.tsukuba02.R2>,
677 2017.
- 678 Nassar, R., Jones, D. B. A., Suntharalingam, P., Chen, J. M., Andres, R. J., Wecht, K. J., Yantosca, R. M., Ku-
679 lawik, S. S., Bowman, K. W., Worden, J. R., Machida, T., and Matsueda, H.: Modeling global atmos-
680 pheric CO₂ with improved emission inventories and CO₂ production from the oxidation of other carbon
681 species, *Geosci. Model Dev.*, 3, 689–716, <https://doi.org/10.5194/gmd-3-689-2010>, 2010.
- 682 Nassar, R., Hill, T. G., McLinden, C. A., Wunch, D., Jones, D. B. A., and Crisp, D.: Quantifying CO₂ emis-
683 sions From Individual Power Plants from Space, *Geophys. Res. Lett.*, 44, 10045– 10053,
684 <https://doi.org/10.1002/2017GL074702>, 2017.
- 685 Notholt, J., Petri, C., Warneke, T., Deutscher, N., Buschmann, M., Weinzierl, C., Macatangay,
686 R., and Grupe, P.: TCCON data from Bremen, Germany, Release GGG2014R0. TCCON data
687 archive, hosted by CaltechDATA, California Institute of Technology, Pasadena, CA, U.S.A.
688 <https://doi.org/10.14291/tcon.ggg2014.bremen01.R0/1149275>, 2017a.
- 689 Notholt, J., Schrems, O., Warneke, T., Deutscher, N., Weinzierl, C., Palm, M., Buschmann, M.,
690 and AWI-PEV Station Engineers: TCCON data from Ny Alesund, Spitzbergen, Norway, Re-
691 lease GGG2014R0. TCCON data archive, hosted by CaltechDATA, California Institute of
692 Technology, Pasadena, CA, U.S.A. <https://doi.org/10.14291/tcon.ggg2014.nyale->
693 [sund01.R0/1149278](https://doi.org/10.14291/tcon.ggg2014.nyalesund01.R0/1149278), 2017b.
- 694 O'Dell, C., Connor, B., Bösch, H., O'Brien, D., Frankenberg, C., Castano, R., Christi, M., Eldering, D.,
695 Fisher, B., Gunson, M., McDuffie, J., Miller, C. E., Natraj, V., Oyafuso, F., Polonsky, I., Smyth, M., Tay-
696 lor, T., Toon, G., Wennberg, P., and Wunch, D.: The ACOS CO₂ retrieval algorithm – Part 1: Description
697 and validation against synthetic observations, *Atmos. Meas. Tech.*, 5, 99–121, <https://doi.org/10.5194/amt->
698 [5-99-2012](https://doi.org/10.5194/amt-5-99-2012), 2012.
- 699 Park, B. C. and Prather, M. J.: CO₂ source inversions using satellite observations of the upper troposphere,
700 *Geophys. Res. Lett.*, 28, 4571–4574, <https://doi.org/10.1029/2001GL013604>, 2001.
- 701 Parrington, M., Palmer, P. I., Henze, D. K., Tarasick, D. W., Hyer, E. J., Owen, R. C., Clerbaux, C., Bowman,
702 K. W., Deeter, M. N., Barratt, E. M., Coheur, P.-F., Hurtmans, D., George, M., and Worden, J. R.: The in-
703 fluence of boreal biomass burning emissions on the distribution of tropospheric ozone over North Amer-
704 ica and the North Atlantic during 2010, *Atmos. Chem. Phys.*, 12, 2077–2098, 2012.
- 705 Patra, P. K., Crisp, D., Kaiser, J. W., Wunch, D., Sasaki, T., Ichii, K., Sekiya, T., Wennberg, P. O., Feist, D. G.,
706 Pollard, D. F., Griffith, D. W. T., Velazco, V. A., De Maziere, M., Sha, M. K., Roehl, C., Chatterjee, A.,



- 707 and Ishijima, K.: The Orbiting Carbon Observa- tory (OCO-2) tracks 2–3 peta-gram increase in carbon
708 release to the atmosphere during the 2014–2016 El Niño, *Sci. Rep.-UK*, 7, 13567,
709 <https://doi.org/10.1038/s41598-017-13459-0>, 2017.
- 710 Peters, W., Jacobson, A. R., Sweeney, C., Andrews, A. E., Conway, T. J., Masarie, K., Miller, J. B., Bruh-
711 wiler, L. M. P., P’etron, G., Hirsch, A. I., Worthy, D. E. J., Werf, G. R. V. D., Randerson, J. T., Wennberg,
712 P. O., Krol, M. C., and Tans, P. P.: An atmospheric perspective on North American carbon dioxide ex-
713 change: CarbonTracker, *P. Natl. Acad. Sci.*, 104, 18925–18930, 2007..
- 714 Peylin, P., Law, R. M., Gurney, K. R., Chevallier, F., Jacobson, A. R., Maki, T., Niwa, Y., Patra, P. K., Peters,
715 W., Rayner, P. J., Rödenbeck, C., van der Laan-Luijkx, I. T., and Zhang, X.: Global atmospheric carbon
716 budget: results from an ensemble of atmospheric CO₂ inversions, *Biogeosciences*, 10, 6699–6720,
717 <https://doi.org/10.5194/bg-10-6699-2013>, 2013.
- 718 Potter, C. S., Randerson, J. T., Field, C. B., Matson, P. A., Vitousek, P. M., Mooney, H. A., and Klooster, S.
719 A.: Terrestrial ecosystem production: A process model based on global satellite and surface data, *Global*
720 *Biogeochem. Cycles*, 7(4), 811–841, <https://doi.org/10.1029/93GB02725>, 1993.
- 721 Rayner, P. J. and O’Brien, D. M.: The utility of remotely sensed CO₂ concentration data in surface source
722 inversions, *Geophys. Res. Lett.*, 28, 175–178, <https://doi.org/10.1029/2000GL011912>, 2001.
- 723 Reuter, M., Buchwitz, M., Hilker, M., Heymann, J., Schneising, O., Pillai, D., Bovensmann, H., Burrows, J.
724 P., Bösch, H., Parker, R., Butz, A., Hasekamp, O., O’Dell, C. W., Yoshida, Y., Gerbig, C., Nehr Korn, T.,
725 Deutscher, N. M., Warneke, T., Notholt, J., Hase, F., Kivi, R., Sussmann, R., Machida, T., Matsueda, H.,
726 and Sawa, Y.: Satellite-inferred European carbon sink larger than expected, *Atmos. Chem. Phys.*, 14,
727 13739–13753, <https://doi.org/10.5194/acp-14-13739-2014>, 2014.
- 728 Reuter, M., Buchwitz, M., Hilker, M., Heymann, J., Bovensmann, H., Burrows, J. P., Houweling, S., Liu, Y.
729 Y., Nassar, R., Chevallier, F., Ciais, P., Marshall, J., and Reichstein, M.: How Much CO₂ Is Taken Up by
730 the European Terrestrial Biosphere?. *Bull. Amer. Meteor. Soc.*, 98, 665–671,
731 <https://doi.org/10.1175/BAMS-D-15-00310.1>, 2017.
- 732 Rienecker, M. M., Suarez, M. J., Todling, R., Bacmeister, J., Takacs, L. and co-authors: The GEOS-5 Data
733 Assimilation System-Documentation of versions 5.0.1 and 5.1.0, and 5.2.0 NASA Tech. Rep. Series on
734 Global Modeling and Data Assimilation, NASA/TM-2008-104606, Vol. 27, 92 pp, 2008.
- 735 Rodgers, C. D.: *Inverse Methods for Atmospheric Sounding: Theory and Practice*, World Scientific Publish-
736 ing Co Inc, Singapore, chapter 2, 2000.
- 737 Saeki, T., Maksyutov, S., Saito, M., Valsala, V., Oda, T., An- dres, R. J., Belikov, D., Tans, P., Dlugokencky,
738 E., Yoshida, Y., Morino, I., Uchino, O., and Yokota, T.: Inverse modeling of CO₂ fluxes using GOSAT
739 data and multi-year ground-based obser- vations, *SOLA*, 9, 45–50, <https://doi.org/10.2151/sola.2013-011>,
740 2013.
- 741 Sherlock, V., Connor, B., Robinson, J., Shiona, H., Smale, D., and Pollard, D.: TCCON data from
742 Lauder, New Zealand, 125HR, Release GGG2014R0. TCCON data archive, hosted by Cal-
743 techDATA, California Institute of Technology, Pasadena, CA, U.S.A.
744 <https://doi.org/10.14291/tcon.ggg2014.lauder02.R0/1149298>, 2017.
- 745 Singh, K., Jardak, M., Sandu, A., Bowman, K., Lee, M., and Jones, D.: Construction of non-diagonal back-
746 ground error covariance matrices for global chemical data assimilation, *Geosci. Model Dev.*, 4, 299–316,
747 <https://doi.org/10.5194/gmd-4-299-2011>, 2011.
- 748 Suntharalingam, P., Jacob, D. J., Palmer, P. I., Logan, J. A., Yantosca, R. M. and co-authors: Improved quan-
749 tification of Chinese carbon fluxes using CO₂/CO correlations in Asian outflow. *J. Geophys. Res.* 109,
750 D18S18, <https://doi.org/10.1029/2003JD004362>, 2004.
- 751 Sussmann, R., and Rettinger, M.: TCCON data from Garmisch, Germany, Release GGG2014R2.
752 TCCON data archive, hosted by CaltechDATA, California Institute of Technology, Pasadena,
753 CA, U.S.A. <https://doi.org/10.14291/tcon.ggg2014.garmisch01.R2>, 2017.
- 754 Takagi, H., Saeki, T., Oda, T., Saito, M., Valsala, V., Belikov, D., Saito, R., Yoshida, Y., Morino, I., Uchino,



- 755 O., Andres, R. J., Yokota, T., and Maksyutov, S.: On the benefit of GOSAT observations to the estimation
756 of regional CO₂ fluxes, SOLA, 7, 161–164, <https://doi.org/10.2151/sola.2011-041>, 2011.
- 757 Tarantola, A.: Inverse Problem Theory and Methods for Model Parameter Estimation, Soc. Industr. App.l
758 Math., Philadelphia, PA, USA, 2004.
- 759 van der Werf, G. R., Randerson, J. T., Giglio, L., Collatz, G. J., Mu, M., Kasibhatla, P. S., Morton, D. C., De-
760 Fries, R. S., Jin, Y., and van Leeuwen, T. T.: Global fire emissions and the contribution of deforestation,
761 savanna, forest, agricultural, and peat fires (1997–2009), Atmos. Chem. Phys., 10, 11707–11735,
762 <https://doi.org/10.5194/acp-10-11707-2010>, 2010.
- 763 Wang, X., Guo, Z., Huang, Y. P., Fan, H. J., and Li, W. B.: A cloud detection scheme for the Chinese carbon
764 dioxide observation satellite (TANSAT). Adv. Atmos. Sci., 34(1), 16–25, [https://doi.org/10.1007/s00376-](https://doi.org/10.1007/s00376-016-6033-y)
765 016-6033-y, 2017.
- 766 Warneke, T., Messerschmidt, J., Notholt, J., Weinzierl, C., Deutscher, N., Petri, C., Grupe, P.,
767 Vuillemin, C., Truong, F., Schmidt, M., Ramonet, M., and Parmentier, E.: TCCON data from
768 Orleans, France, Release GGG2014R0. TCCON data archive, hosted by CaltechDATA, Cali-
769 fornia Institute of Technology, Pasadena, CA, U.S.A.
770 <https://doi.org/10.14291/tcon.ggg2014.orleans01.R0/1149276>, 2017.
- 771 Wennberg, P. O., Roehl, C., Wunch, D., Toon, G. C., Blavier, J.-F., Washenfelder, R., Keppel-Aleks, G., Al-
772 len, N., and Ayers, J.: TCCON data from Park Falls, Wisconsin, USA, Release GGG2014R1. TCCON
773 data archive, hosted by CaltechDATA, California Institute of Technology, Pasadena, CA, U.S.A.
774 <http://doi.org/10.14291/tcon.ggg2014.parkfalls01.R1>, 2017.
- 775 Wennberg, P. O., Wunch, D., Roehl, C., Blavier, J.-F., Toon, G. C., Allen, N., Dowell, P., Teske, K., Martin,
776 C., and Martin, J.: TCCON data from Lamont, Oklahoma, USA, Release GGG2014R1. TCCON data ar-
777 chive, hosted by CaltechDATA, California Institute of Technology, Pasadena, CA, U.S.A.
778 <https://doi.org/10.14291/tcon.ggg2014.lamont01.R1/1255070>, 2017. Wilkerson, J. T., Jacobson, M. Z.,
779 Malwitz, A., Balasubramanian, S., Wayson, R., Fleming, G., Naiman, A. D., and Lele, S. K.: Analysis of
780 emission data from global commercial aviation: 2004 and 2006, Atmos. Chem. Phys., 10, 6391–6408,
781 <https://doi.org/10.5194/acp-10-6391-2010>, 2010.
- 782 Wunch, D., Wennberg, P. O., Toon, G. C., Connor, B. J., Fisher, B., Osterman, G. B., Frankenberg, C., Man-
783 drake, L., O'Dell, C., Ahonen, P., Biraud, S. C., Castano, R., Cressie, N., Crisp, D., Deutscher, N. M.,
784 Eldering, A., Fisher, M. L., Griffith, D. W. T., Gunson, M., Heikkinen, P., Keppel-Aleks, G., Kyrö, E.,
785 Lindenmaier, R., Macatangay, R., Mendonca, J., Messerschmidt, J., Miller, C. E., Morino, I., Notholt, J.,
786 Oyafuso, F. A., Rettinger, M., Robinson, J., Roehl, C. M., Salawitch, R. J., Sherlock, V., Strong, K., Suss-
787 mann, R., Tanaka, T., Thomp- son, D. R., Uchino, O., Warneke, T., and Wofsy, S. C.: A method for evalu-
788 ating bias in global measurements of CO₂ total columns from space, Atmos. Chem. Phys., 11, 12317–
789 12337, <https://doi.org/10.5194/acp-11-12317-2011>, 2011.
- 790 Wunch, D., Wennberg, P. O., Osterman, G., Fisher, B., Naylor, B., Roehl, C. M., O'Dell, C., Mandrake, L.,
791 Viatte, C., Kiel, M., Griffith, D. W. T., Deutscher, N. M., Velasco, V. A., Notholt, J., Warneke, T., Petri,
792 C., De Maziere, M., Sha, M. K., Sussmann, R., Rettinger, M., Pollard, D., Robinson, J., Morino, I.,
793 Uchino, O., Hase, F., Blumenstock, T., Feist, D. G., Arnold, S. G., Strong, K., Mendonca, J., Kivi, R.,
794 Heikkinen, P., Iraci, L., Podolske, J., Hillyard, P. W., Kawakami, S., Dubey, M. K., Parker, H. A., Sepul-
795 veda, E., Garcia, O. E., Te, Y., Jeseck, P., Gunson, M. R., Crisp, D., and Eldering, A.: Comparisons of the
796 Orbiting Carbon Observatory-2 (OCO-2) XCO₂ measurements with TCCON, At- mos. Meas. Tech., 10,
797 2209–2238, [https://doi.org/10.5194/amt-](https://doi.org/10.5194/amt-10-2209-2017)
10-2209-2017, 2017.
- 798 Yang, D. X., Liu, Y., Cai, Z. N., Chen, X., Yao, L., and Lu, D. R.: First global carbon dioxide maps produced
799 from TanSat measurements. Adv. Atmos. Sci., 35(6), 621–623, [https://doi.org/10.1007/s00376-018-7312-](https://doi.org/10.1007/s00376-018-7312-6)
800 6, 2018.
- 801 Zhu, C., Byrd, R. H., Lu, P. and Nocedal, J.: L-BFGS-B: algorithm 778: L-BFGS-B, FORTRAN routines for
802 large scale bound constrained optimization. ACM Trans. Math. Softw. 23(4), 550_560.
803 <https://doi.org/10.1145/279232.279236>, 1997.